Check for updates

Synthesis of highly sensitive disordered porous SnO_2 aerogel composite material by the chemical deposition method: synergistic effect of a layer of CuO thin film†

Tian-tian Li,[a] Ren-rong Zheng,[a] Hui Yu, [ID] *[a] Ying Yang, [ID] *[ab] Ting-ting Wang[a] and Xiang-ting Dong [ID] [a]

In this study, a new chemical deposition method was innovatively used to prepare disordered porous CuO/SnO_2 aerogel composite material (CuO/SnO_2-ACM). The CuO/SnO_2-ACM was a p–p combined structure semiconductor, with a layer of CuO thin film formed on the surface of disordered porous SnO_2 aerogel matrix material (SnO_2-AMM). For the first time, the aerogel technology was used to prepare the porous tin dioxide material. The metal Cu was deposited on the surface of the SnO_2-AMM to form the film. Finally, the sample was calcined, and a layer of CuO thin film was formed on the surface of the SnO_2-AMM. Compared with the SnO_2-AMM, the prepared CuO/SnO_2-ACM showed enhanced sensitivity to NO_x gas at the room temperature. When the NO_x concentration was 100 ppm, the response reached 74%, and the response time was only 7.0 s. A detection limit to NO_x gas of 1 ppm could be reached, with a response and response time of 15% and 26 s, respectively. In addition, excellent restorability and superior selectivity could be observed in the prepared sensor. The excellent gas sensing properties of the prepared CuO/SnO_2-ACM can be attributed to the unique structure and synergistic effect of CuO thin film.

1. Introduction

There are abundant harmful gases in the environment, such as acetone, sulfur dioxide, carbon monoxide, nitrogen oxides and so on. Environmental pollution has become a very critical problem in recent years.[1] In order to control this situation, most of the semiconductor gas sensors are made from MOS (metal oxide semiconductor), which are widely used to detect, monitor, control the toxic and harmful gases. They show a good application prospect in environmental science.[2–9] As a broad-spectrum semiconductor, SnO_2 has been extensively studied as a gas sensing material.[10] Compared with other semiconductor gas sensitive materials, SnO_2 has many advantages, such as simple manufacture, fast response and recovery times, a high sensitivity to oxidation gases, etc.[11–13] Different methods can be used to prepare various structural SnO_2 materials, including surface modification of materials and doping of materials to improve the their performance for gas sensing.[14] The sensing properties of a gas sensor are greatly influenced by

the microstructures, grain size, morphologies, and temperature.[15,16] SnO_2 materials have been prepared with different structures,[17] such as nanotubes,[18] nanorods,[19] nanosheets,[20] nanofibers,[21] hollow spheres,[22] hierarchical flowerlike nanostructures,[23] hollow porous microcubes, etc.[24–28] With the deepening of the research, it is found that the gas sensing properties of the SnO_2-based composite materials are much higher than those of pure SnO_2. Mishra et al.[9] described Cu-doped SnO_2 nanoparticles, which were synthesized by a co-precipitation method, and were then investigated as a formaldehyde sensing material. The 1.5 wt% Cu-doped SnO_2 showed a selective high response (~80%) to 50 ppm concentration of formaldehyde at 200 °C. Qin et al.[15] prepared Nd-doped SnO_2 nanorods by a substrate-free hydrothermal route of using sodium stannate and sodium hydroxide at 210 °C. The Nd-doped SnO_2 nanorods with an optimized Nd doping level of 3.0 wt% exhibited an excellent sensing response toward alcohol at 260 °C. Li et al.[2] demonstrated Cu^{2+}/Au co-doped SnO_2 nanofibers by electrospinning method, which were used to detect acetylene (C_2H_2) at 160 °C.

CuO was reported to have outstanding promotive action.[29] CuO/SnO_2 heterostructures revealed an extraordinary performance in sensors.[30,31] The p-type CuO and n-type SnO_2 form a p–n junction with a depletion zone. Some studies reported a highly sensitive CuO–SnO_2 composite nano-fibers for H_2S detection.[32,33] Considerable efforts have been focused on

[a]School of Chemistry & Environmental Engineering, Changchun University of Science and Technology, Changchun 130022, P. R. China. E-mail: yh2001101@163.com; yangying0807@126.com; Fax: +86-431-85383815; Tel: +86-431-85583008

[b]Key Laboratory of Functional Inorganic Material Chemistry, Heilongjiang University, Ministry of Education, Harbin 150080, P. R. China

† Electronic supplementary information (ESI) available. See DOI: 10.1039/c7ra06415b

fabricating of the one-dimensional nano materials *via* thermal oxidation, thermal evaporation, hydrothermal process and electro-spinning.[30,34] Li *et al.* synthesized Cu-doped SnO_2 nano fibers *via* electro-spinning, and the rapid response to ethanol was reported.[35] Shao *et al.*[36] reported p-CuO (particle)/n-SnO_2 (nanowire) heterostructures devices and their application as H_2S sensors. CuO/SnO_2 films were one of the most promising for detecting H_2S.[30,37,38] The Cu element was dispersed either in the form of islands or as a continuous layer on the surface of the SnO_2 film, which showed a reasonably strong sensor response to H_2S.[34] Toan *et al.* reported the H_2S gas sensors using SnO_2 thin films sensitized with CuO islands.[39] Choi *et al.* proposed that CuO loaded SnO_2 hollow spheres showed almost negligible humidity dependence of sensor signal even under highly humid (RH of 80%) atmosphere as well as ultrahigh response and selectivity to sub-ppm H_2S.[40] Multilayered SnO_2–CuO thin films were also fabricated for highly sensitive H_2S sensing.[41]

Porous materials are used in gas sensitive field which can be attributed to their effective surface area and porosity.[42] The porous structures can increase the specific surface areas of the materials, effectively. The large specific surface area means that the atoms are located on the surface, and participate in surface reactions. The porous materials can provide the more active sites, improve the surface adsorption capacity to gases, and make the gases spread into the prepared material, which finally enhance the gas-sensing properties of samples.[43] Therefore, the preparation of porous SnO_2-based composite materials is an obvious trend. It has been reported that the mesoporous structure can provide high surface area and well-defined porous architecture for high gas response and rapid gas responding kinetics.[44] A series of porous SnO_2 semiconductor materials were widely used for gas sensors.[45] Guo *et al.*[46] have also investigated the gas sensing performances of mesoporous SnO_2 towards toxic gases with a different reducing ability. The ordered periodical structures and large specific surface area allow for improved performances.[47–51] The ordered 2D mesoporous SnO_2 structures with high crystallinity and large surface area have been successfully prepared by using nanocasting method for detecting a variety of gases.[52] Compared with the ordered porous materials, the disordered porous SnO_2 aerogel composite material is very meaningful. The disordered porous SnO_2 aerogel has the higher porosity, which has the higher gas-sensing properties. Until now, it is without reported about the disordered porous SnO_2 aerogel.

In this study, the disordered porous CuO/SnO_2 aerogel composite materials with excellent gas sensing properties were successfully prepared by the chemical deposition method. The study was quite different from the past reported articles in preparation and gas sensing. First, the aerogel technology was used to prepare the porous tin dioxide material. Second, the metal Cu was deposited on the surface of the prepared porous SnO_2 material to form the film, which was calcined, and a layer of CuO thin film was formed on the surface of the prepared porous SnO_2 material. The structure of the prepared material was characterized by X-ray diffraction (XRD), scanning election microscope (SEM), transmission electron microscopy (TEM), N_2 adsorption–desorption method and energy dispersive X-ray

spectrometer (EDS). The gas sensing properties of CuO/SnO_2-ACM to NO_x gas were investigated. The synthesized CuO/SnO_2-ACM was provided with excellent gas sensing properties, high sensitivity, good stability, fast response time.

2. Experimental section

All chemicals used in this work were of analytical grade, and without further purification. Tin(II) chloride dihydrate ($SnCl_2$·$2H_2O$, A.R.) was purchased from Xilong Chemical Research Institute in China. Tetraethyl silicate (TEOS, A.R.), *n*-hexane (A.R.) and sodium hydroxide (NaOH, A.R.) were purchased from Beijing Chemical Works Research Institute in China. Potassium sodium tartrate tetrahydrate ($C_4H_4O_6KNa$·$4H_2O$, A.R.) was purchased from Tianjin Guangfu Technology Development Co., Ltd in China. Formaldehyde solution (HCHO, A.R.) was purchased from Tianjin Fuchen Chemical Reagents Factory in China. Ethylene diamine tetraacetic acid disodium (EDTA-2Na, A.R.) was purchased from Shenyang Reagent Factory in China. Copper(II) sulfate pentahydrate ($CuSO_4$·$5H_2O$, A.R.) was purchased from Sinopharm Chemical Reagent Co., Ltd in China. Ethanol and deionized water were used for all process of washing and dissolution.

2.1. Synthesis

Disordered porous SnO_2 aerogel matrix material (SnO_2-AMM). 0.05 mol $SnCl_2$·$2H_2O$ was weighed accurately, and put into a small beaker. 6.2 mL anhydrous ethanol was added into the beaker, which was stirred for 30 min in room temperature. 3.8 mL deionized water was added slowly, and the mixture was stirred for 2–3 h to obtain uniform mixed solution in room temperature. 5.7 mL tetraethyl silicate (TEOS, 99.5%) was added into the beaker slowly, which was stirred, and was formed Sn/Si composite gel bulk. The sample was aged for 24 h in room temperature, and then was aged at 70 °C for 2 days. The sample was soaked into the *n*-hexane for 2 days under 50 °C. The wet gel bulk was washed using water and ethanol, and was dried in room temperature. The sample was soaked into NaOH solution (pH = 13), and stirred for 30 min under 50 °C. The sample was filtered, washed, dried and calcined at 550 °C, and the purpose sample was obtained.

Disordered porous CuO/SnO_2 aerogel composite material (CuO/SnO_2-ACM). A certain amount of $CuSO_4$·$5H_2O$, EDTA-2Na and $C_4H_4O_6KNa$·$4H_2O$ were added into 250 mL of deionized water, and the mixture was stirred to form solution at 50 °C. At room temperature, the pH of the solution was adjusted to 12.5 with NaOH. The disordered porous SnO_2 material was added in the solution, and then the HCHO was added. The mixture was stirred for 1 h, and then was filtered, washed, dried and calcined at 500 °C for 4 h to form the CuO film on the surface of the prepared SnO_2 aerogel. Finally, the disordered porous CuO/SnO_2 aerogel composite material was obtained.

2.2. Characterizations

The crystallographic structures of the prepared CuO/SnO_2-ACM was determined using X-ray diffraction (XRD, Siemens D5005,

with high-intensity Cu-Kα radiation with a wavelength of 1.5418 Å). The morphology and composition of the prepared materials were investigated by scanning election microscope (SEM, JEOL JSM-5600L) with an energy dispersive X-ray spectrometer (EDS). The microstructures of the prepared materials were investigated by transmission electron microscopy (TEM, JEOL 2010 TEM instrument). Physical adsorption of nitrogen was performed on a Micromeritics ASAP2010M volumetric adsorption analyzer at 77 K. The CuO/SnO$_2$-ACM was degassed in vacuum at 573 K for 12 h before measurement. Surface area was calculated based on the BET model, while pore size was computed using the BJH method.

2.3. Gas sensing measurements

An interdigitated Au electrode (7 × 5 × 0.25 mm) was selected for gas sensing detection, and the finger spacing was 20 μm. The prepared CuO/SnO$_2$-ACM was dispersed in ethanol to form a suspension. Then, the suspension was coated onto the electrode. It was dried at 60 °C for 1 h to obtain a thin film gas sensor.

The responses of the prepared gas sensor to the different concentrations NO$_x$ gas were performed. The sensor was placed in a static flow system, which has only one inlet and one outlet. The test chamber needed to be pumped for 2 min to let the sample room full of air, and obtain the stable absorption film. A syringe was used to inject gas into the sample room, and observed the change of resistance. The response is signed as S, which is calculated according to reported equation (eqn (1)):[53,54]

$$S\ (\%) = [(R_g - R_a/R_a)] \times 100 \tag{1}$$

where R_a and R_g are the resistances of the prepared gas sensor in air and the test gas (NO$_x$), respectively. The response and recovery times are defined as the time needed for 85% of total resistance change on exposure in test gas and air, respectively.

3. Results and discussion

3.1. Structural characterizations

Fig. 1 showed the XRD patterns of the prepared SnO$_2$-AMM and CuO/SnO$_2$-ACM. In Fig. 1(a), the diffraction peaks at 26.8°, 34.3°, 37.9°, 52.1°, 54.7°, 62.9°, 64.3°, 71.4° and 78.7° could be assigned to (110), (101), (200), (211), (220), (310), (301), (202) and (321) planes of SnO$_2$ with tetragonal rutile structure (PDF# 41-1445). In Fig. 1(b), the diffraction peaks at 32.5°, 35.4° and 38.9° could be assigned to (110), (002) and (200) planes of CuO with monoclinic system structure, which was consistent with the data format of the standard data file PDF# 48-1548. All of the diffraction patterns were attributed to the characteristic peaks of CuO and SnO$_2$, and no other diffraction peak was observed. It showed that the CuO has been successfully coated on the surface of the SnO$_2$-AMM. It could be proved that the disordered porous CuO/SnO$_2$ aerogel composite material could be obtained by the chemical deposition method. From the Fig. 1, the peaks of the SnO$_2$ and CuO were broadened. It could be attributed to the lower crystallization degrees of the sample, which was the
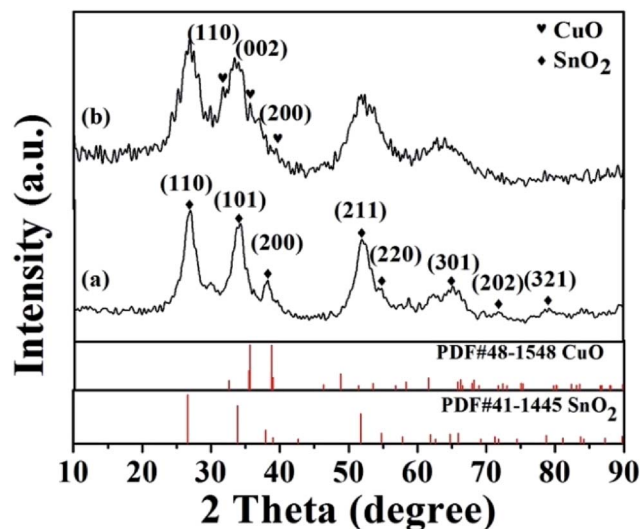

Fig. 1 XRD patterns of (a) SnO$_2$-AMM, and (b) CuO/SnO$_2$-ACM.

defect of sol–gel method, and the introduced CuO further reduced the crystallization degrees.

The morphology and microstructure of the prepared materials were determined using SEM. Fig. 2(a) and (b) showed the SEM images of the prepared CuO/SnO$_2$-ACM sample. Fig. 2(a) indicated that the morphology of the CuO/SnO$_2$-ACM was cluster like loosened structure in the lower magnification. The clusters were consisted of irregular sphere particles, and the diameters of those sphere particles were ranges from 100–200 nm in the Fig. 2(b). Fig. 2(c) showed the SEM images of the prepared Cu/SnO$_2$ sample, which showed also the cluster like structure. The clusters were consisted of irregular sphere particles, which showed the serious agglomeration. In order to research the microstructure of the prepared materials, the typical TEM images were collected, which was taken with the beam direction parallel to the pores, the result were shown in Fig. 2(d). It could be clearly seen that its surfaces distributed the disordered loosened porous, which was easier to adsorb gas. The TEM image of Cu/SnO$_2$ sample was showed in Fig. 2(e). It could be clearly seen that its surfaces distributed the disordered porous structure, whose poriness was lower than CuO/SnO$_2$-ACM sample. The composition of the CuO/SnO$_2$-ACM was determined from the EDS spectrum in the Fig. 2(f). The signals of Si and C were introduced from the silicon slice and conducting resin, which were used in the test procedure. The prepared CuO/SnO$_2$-ACM was composed of Cu, Sn and O species. From EDS analysis results, the atomic percentages of Sn, O and Cu were 55.8 wt%, 40.3 wt% and 3.9 wt%, respectively.

Fig. 3 showed the low temperature nitrogen adsorption–desorption isotherms of the prepared SnO$_2$-AMM (Fig. 3(a)) and CuO/SnO$_2$-ACM (Fig. 3(b)). The isotherms belonged to the typical irreversible IV type isotherms with H1 hysteresis loop, which was the feature of the cylindrical pore. From Fig. 3, the adsorbing capacity gently increased at low pressure, it could be due to which the N$_2$ molecules were absorbed on the inner surface of the pores in the form of single layer to multi-layer. In
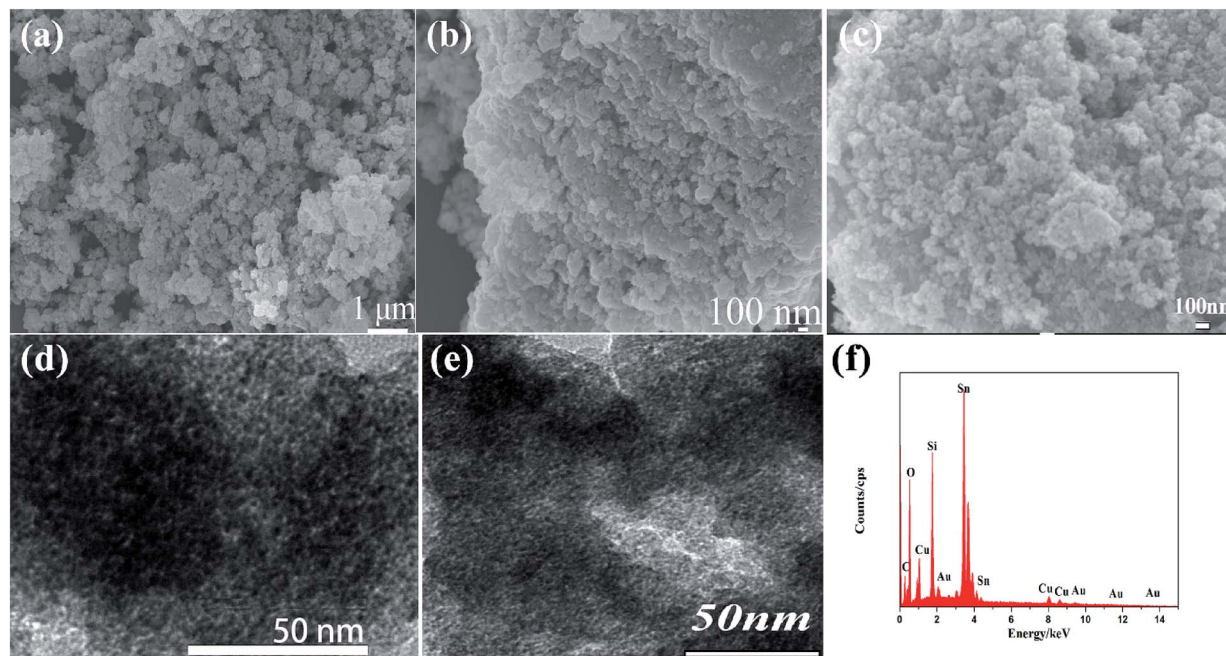
Fig. 2 (a) and (b) SEM images of the CuO/SnO$_2$-ACM. (c) SEM images of the Cu/SnO$_2$. (d) and (e) TEM image of the CuO/SnO$_2$-ACM and Cu/SnO$_2$. (f) EDS spectrum of the CuO/SnO$_2$-ACM.
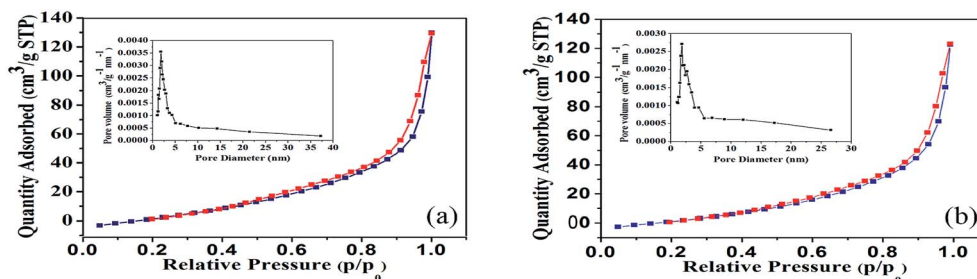

Fig. 3 Nitrogen adsorption–desorption isotherm and pore diameter distribution of (a) SnO$_2$-AMM, and (b) CuO/SnO$_2$-ACM.

the high pressure, capillary condensations were happened, the isotherms rose rapidly, and the lag phenomenon was observed. The steep adsorption hysteresis associated with the narrow pore size distribution (the illustrations of the Fig. 3), which indicated that the pores of the samples were homogeneous. The specific surface area and pore size distribution were calculated by BET method and BJH model, respectively. The specific surface area, the most probable pore diameter, pore volume of the SnO$_2$-AMM and CuO/SnO$_2$-ACM were 74.935 and 66.627 m^2 g^{-1}, 1.80 and 1.60 nm, 0.228 and 0.217 cm^3 g^{-1}, respectively. The three values of the CuO/SnO$_2$-ACM sample were smaller than the SnO$_2$-AMM. It illustrated that the CuO was coated on the surface of the SnO$_2$-AMM, and formed a layer of CuO thin film on the surface of SnO$_2$-AMM.

3.2. Gas sensing properties

At room temperature, the gas sensing properties of the prepared materials to nitrogen oxides (NO$_x$) were tested by thin film sensors, which were prepared using the SnO$_2$-AMM and CuO/

SnO$_2$-ACM. Fig. 4(a) and (c) were the response–recovery curves of the SnO$_2$-AMM and CuO/SnO$_2$-ACM gas sensor during cyclic exposure in different concentrations NO$_x$, respectively. The resistance sharply decreased, and gradually reached the minimum resistance in a very short period of time when NO$_x$ gas was injected into the sample room. After the gas was withdrawn, the resistance was quickly recovered to the previous value. It was the typical of the p-type semiconductor, and the CuO/SnO$_2$-ACM was a p–p combined structure semiconductor. From the Fig. 4(a) and (c), the prepared thin film sensor had a better response to the NO$_x$ gas, and the sensor could be repeated without a noticeable properties decrease. It could be seen that the detection limit of the CuO/SnO$_2$-ACM sensor (1 ppm) was lower than SnO$_2$-AMM sensor (5 ppm). Its recovery performance was also much better than SnO$_2$-AMM sensor.

Fig. 4(b) and (d) showed the response and response time curve of the SnO$_2$-AMM and CuO/SnO$_2$-ACM sensor towards the different concentration NO$_x$ at the room temperature, respectively. With the NO$_x$ concentration decrease, the responses were
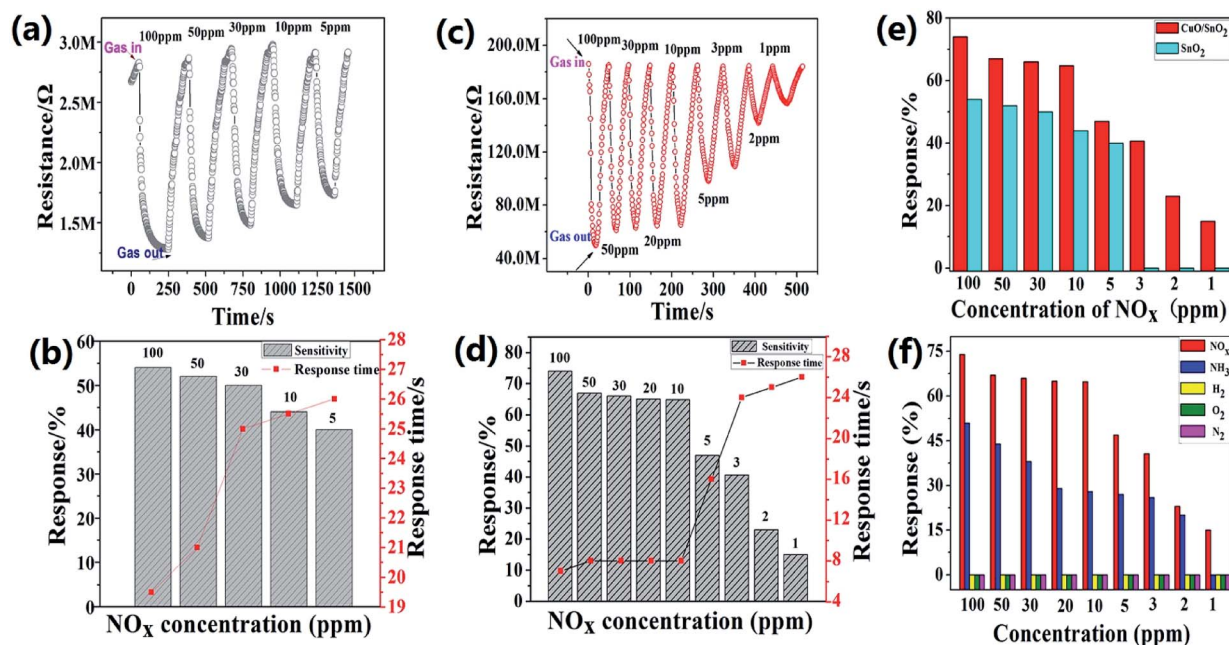
Fig. 4   (a) and (c) The response–recovery curves of SnO_2-AMM and CuO/SnO_2-ACM gas sensor during cyclic exposure in different concentrations NO_x. (b and d) Response and response time curve of SnO_2-AMM and CuO/SnO_2-ACM gas sensor in the different concentration NO_x at the room temperature. (e) The gas sensing performance bar graphs of SnO_2-AMM and CuO/SnO_2-ACM gas sensor. (f) The gas response bar graphs of CuO/SnO_2-ACM sensor in different gases (NO_x, NH_3, H_2, O_2, N_2).

also reducing. With the NO_x concentration increase, the response time decreased. The concrete data was shown in ESI Table S1.† In Fig. 4(b), the response reached a maximum value of 54%, and the response time was 19.5 s when the NO_x gas concentration was 100 ppm. From 100 to 5 ppm NO_x concentration, the response time of the SnO_2-AMM sensor ranged from 19.5 to 26 s. The minimum detection limit of the SnO_2-AMM sensor was 5 ppm, whose response and response time were 40% and 26 s, respectively. In Fig. 4(d), the response reached a maximum value of 74%, and the response time was only 7 s when the NO_x gas concentration was 100 ppm. From 100 to 1 ppm NO_x concentration, the response time of the CuO/SnO_2-ACM sensor ranged from 7 to 26 s. The minimum detection limit of the CuO/SnO_2-ACM sensor was 1 ppm, whose response and response time were 15% and 26 s, respectively. There was a sudden jump in response time when the NO_x concentration decreases from 10 to 5 and then 3 ppm. In porous materials, the gas adsorption capacity is connected with the gas partial pressures. At low partial pressures, the adsorption is mainly monolayer adsorption, the capillary condensation cannot occur. The adsorption is multilayer adsorption when the relative pressure increases to the capillary condensation occurring, and adsorptive quantity sharply increases (as Fig. 3). In this study, the gas adsorption capacity sharply declined when the NO_x gas concentration reduced under 10 ppm, which led to response and response time a sudden jump. The gas sensing performance comparison bar chart of the SnO_2-AMM and CuO/SnO_2-ACM sensor was shown in Fig. 4(e). It proved that the response and response time of the CuO/SnO_2-ACM sensor were far superior to the SnO_2-AMM sensor.

The gas selectivity is a very important factor for the application of the sensor. Fig. 4(f) showed the gas response bar graphs of the CuO/SnO_2-ACM sensor in different gases (NO_x, NH_3, H_2, O_2, N_2). The concrete data could be found in ESI Table S2.† It showed that the response of the CuO/SnO_2-ACM thin film sensor to NO_x was much higher than the other gases at the same gas concentration. The response reached a maximum value of 74% when the NO_x gas concentration was 100 ppm. For the same NH_3 gas concentration, the maximum response was only 54%. It all know, NH_3 is a reductive gas, NO_2 is an oxidizing gas, and their detection effects have the much bigger difference, the similar result has been obtained in the past research.[55] The responses of other gases were closer to 0%. It proved that the CuO/SnO_2-ACM sensor had the better selectivity to NO_x.

3.3.   Sensing mechanism

As Fig. 4(c), the resistance of the sample sharply decreases when NO_x gas is injected into the sample room, which is the typical characteristic of p-type semiconductors. Therefore, the prepared CuO/SnO_2-ACM is a p–p type metal-oxide semiconductor. Fig. 5 is the microstructure schematic diagram and corresponding sensing mechanism of the CuO/SnO_2-ACM sensor. From Fig. 5, the oxygen (O_2) will be chemisorbed, and capture some electrons from the conduction band of SnO_2 material when the thin film sensor is exposed in the air ambient. It can form an electron depletion layer on the surface of the CuO/SnO_2-ACM sensor, the O_2^-, O^- and O^{2-} species will be created, and they form a follow chemical equilibrium with each other:
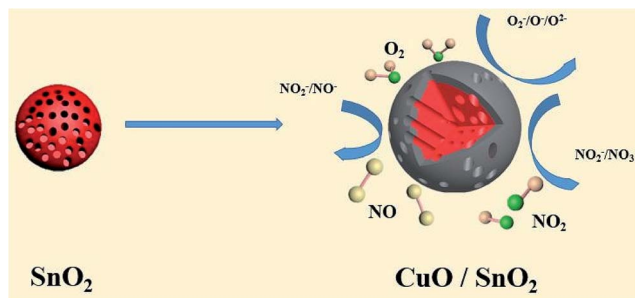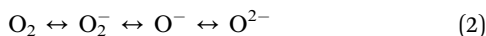
Fig. 5 The microstructure schematic diagram and corresponding sensing mechanism of CuO/SnO$_2$-ACM sensor.

$$O_2 \leftrightarrow O_2^- \leftrightarrow O^- \leftrightarrow O^{2-} \qquad (2)$$

This is the reason why the resistance tends to be stable.[56,57] This system has the better catalytic activity in the CuO/SnO$_2$-ACM sensor. The NO$_x$ gas molecules are oxidized when the thin film sensor is exposed into the oxidation type gas (NO$_x$), which leads that the oxygen ions on the sensor surface are continuously reduced. At the same time, the exhausted electrons are fed back into the conductance band of the CuO/SnO$_2$-ACM, which leads to the decrease of the resistance, and produce of the electrical signals. This reaction between adsorbed oxygen and NO$_x$ gas can be described as the following eqn (3) and (4):

$$NO_2 + e^- \rightarrow NO_2^-/NO + e^- \rightarrow NO^- \qquad (3)$$

$$NO_2 + O^- \rightarrow NO_3^-/NO + O^- \rightarrow NO_2^- \qquad (4)$$
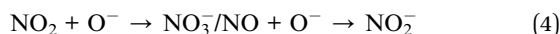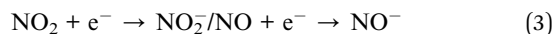
Detailed process can be known through the schematic diagram in the Fig. 5. After filling in the NO$_x$ gas, the resistance of the CuO/SnO$_2$-ACM sensor decreases sharply (Fig. 5). The thin film sensor is exposed to the air again when the NO$_x$ gas is drowned out, and the resistance is quickly restored to its original value.[54,58–60] The above is the principle of the gas sensing performance test.

It is well known that the gas-sensing performance of the sensor is related to the structure of the gas sensing material. The larger specific surface area provides the more gas adsorption sites, the faster response to the gas, the better the gas sensing performance. In this study, the porous structures can effectively increase the specific surface area of the material. Material with high porosity structure can make the gas reach the gas sensitive material effectively and quickly, and a series of reactions occur effectively and quickly. It also can improve the response, response and recovery time of the sensing material.

In this study, the response towards NO$_x$ is largely promoted by the CuO film. The CuO/SnO$_2$-ACM is p–p combined structure semiconductor gas sensor. It bases on the compensation-feedback principle of two different sensors. In Fig. 5, this particular type of semiconductor sensor can effectively improve the response of the sensor and the selectivity toward gas, which can be due to p–p transition layer formation. Cu^{2+} (0.073 nm) ion radius is close to Sn^{4+} (0.069 nm), which makes the nodes replace happen, the grain size decrease, and it does not cause

serious lattice mismatch. It is well known that the smaller the grain size leads to the more active sites on the surface, which increases the response activity. In addition, Cu^{2+} ions occupy the position of Sn^{4+} ion, provide electrons, and the more free electrons participate in the gain and loss electronic of the reaction. It can produce the more oxygen adsorption centers, and increase the number of adsorbed oxygen. Therefore, the porous CuO/SnO$_2$-ACM has the higher response. The prepared CuO/SnO$_2$-ACM will have a great development space in the gas sensor field, and there is a great research value.

4. Conclusions

This study presents a method to prepare the disordered porous CuO/SnO$_2$ aerogel composite material, which is the chemical deposition method. The prepared CuO/SnO$_2$-ACM is a p–p combined structure semiconductor, a layer of CuO thin film is formed on the surface of the SnO$_2$-AMM. The synthesized CuO/SnO$_2$-ACM appears excellent gas sensing properties, the higher and faster response. At room temperature, its response is up reached to 74%, and the response time is only 7 s in 100 ppm NO$_x$ gas. The detection limit to NO$_x$ gas is only 1 ppm, and the corresponding response and response time are 15% and 26 s, respectively. The prepared CuO/SnO$_2$-ACM gas-sensing material has an admirable detection performance and the better selectivity to NO$_x$ gas. The porous gas sensitive materials with high porosity has excellent gas sensing properties, and has the much better development prospects in the gas sensors field.

Conflicts of interest

There are no conflicts to declare.

Acknowledgements

References

1 R. J. Lu, W. Zhou, K. Y. Shi, Y. Yang, L. Wang, K. Pan, C. G. Tian, Z. Y. Rena and H. G. Fu, *Nanoscale*, 2013, **5**, 8569–8576.

2 Z. Y. Li, X. G. Wang and T. Lin, *J. Mater. Chem. A*, 2014, **2**, 13655–13660.

3 S. F. Shao, H. Y. Wu, F. Jiang, S. M. Wang, T. Wu, Y. T. Lei, R. Koehn and W. F. Rao, *RSC Adv.*, 2016, **6**, 22878–22888.

4 S. F. Shao, H. Y. Wu, S. M. Wang, Q. L. Hong, R. Koehn, T. Wu and W. F. Rao, *J. Mater. Chem. C*, 2015, **3**, 10819–10829.

5 H. Nguyen and S. A. El-Safty, *J. Phys. Chem. C*, 2011, **115**, 8466–8474.

6 S. Li, T. Liu, Y. Zhang, W. Zeng, F. Pan and X. Peng, *Mater. Lett.*, 2015, **143**, 12–15.

7 W. Q. Li, S. Y. Ma, J. Luo, Y. Z. Mao, L. Cheng, D. J. Gengzang, X. L. Xu and S. H. Yan, *Mater. Lett.*, 2014, **132**, 338–341.

8 I. Lee, S.-J. Choi, K.-M. Park, S. S. Lee, S. Choi, I.-D. Kim and C. O. Park, *Sens. Actuators, B*, 2014, **197**, 300–307.

9 R. K. Mishra, A. Kushwaha and P. P. Sahay, *RSC Adv.*, 2014, **4**, 3904–3912.

10 Q. Yan, S. Tao and H. Toghiani, *Talanta*, 2009, **77**, 953–961.

11 K. P. Gattu, K. Ghule, A. A. Kashale, V. B. Patil, D. M. Phase, R. S. Mane, S. H. Han, R. Sharrna and A. V. Ghule, *RSC Adv.*, 2015, **5**, 72849–72856.

12 S. F. Bamsaoud, S. B. Rane, R. N. Karekar and R. C. Aiyer, *Sens. Actuators B*, 2011, **153**(2), 382–391.

13 Z. Lou, L. Wang, R. Wang, T. Fei and T. Zhang, *Solid-State Electron.*, 2012, **76**, 91–94.

14 M. X. Chen, C. C. Zhang, L. Z. Li, Y. Liu, X. C. Li, X. Y. Xu, F. L. Xia, W. Wang and J. P. Gao, *ACS Appl. Mater. Interfaces*, 2013, **5**(24), 13333–13339.

15 G. Qin, F. Gao, Q. Jiang, Y. Li, Y. Liu, L. Luo, K. Zhao and H. Zhao, *Phys. Chem. Chem. Phys.*, 2016, **18**, 5537–5549.

16 Z. P. Li, Q. Q. Zhao, W. L. Fan and J. H. Zhan, *Nanoscale*, 2011, **3**, 1646–1652.

17 A. Katoch, J.-H. Kim, Y. J. Kwon, H. W. Kim and S. S. Kim, *ACS Appl. Mater. Interfaces*, 2015, **7**(21), 11351–11358.

18 P. Sun, L. You, Y. F. Sun, N. K. Chen, X. B. Li, H. B. Sun, J. Ma and G. Y. Lu, *CrystEngComm*, 2012, **14**, 1701–1708.

19 S. Wang, J. Yang, H. Zhang, Y. Wang, X. Gao, L. Wang and Z. Zhu, *Sens. Actuators, B*, 2015, **207**(A), 83–89.

20 T. Tao, L. He, J. Li and Y. Zhang, *Mater. Lett.*, 2015, **138**, 45–47.

21 L. Wang, J. Deng, Z. Lou and T. Zhang, *J. Mater. Chem. A*, 2014, **2**, 10022–10028.

22 Y. H. Cho, X. Liang, Y. C. Kang and J.-H. Lee, *Sens. Actuators, B*, 2015, **207**(A), 330–337.

23 L. L. Wang, T. Fei, Z. Lou and T. Zhang, *ACS Appl. Mater. Interfaces*, 2011, **3**(12), 4689–4694.

24 J. R. Huang, L. Y. Wang, C. P. Gu and J.-J. Shim, *Mater. Lett.*, 2014, **136**, 371–374.

25 J. R. Huang, L. Y. Wang, C. P. Gu, M. H. Zhai and J. H. Liu, *CrystEngComm*, 2013, **15**, 7515–7521.

26 H. J. Song, X. H. Jia, H. Qi, X. F. Yang, H. Tang and C. Y. Min, *J. Mater. Chem.*, 2012, **22**, 3508–3516.

27 G. X. Ma, R. J. Zou, L. Jiang, Z. Y. Zhang, Y. F. Xue, L. Yu, G. S. Song, W. Y. Li and J. Q. Hu, *CrystEngComm*, 2012, **14**, 2172–2179.

28 Q. Z. Jiao, M. Fu, C. You, Y. Zhao and H. S. Li, *Inorg. Chem.*, 2012, **51**, 11513–11520.

29 J. H. Jeun and S. H. Hong, *Sens. Actuators, B*, 2010, **151**, 1–7.

30 I. S. Hwang, J. K. Choi, S. J. Kim, K. Y. Dong, J. H. Kwon, B. K. Ju and J. H. Lee, *Sens. Actuators, B*, 2009, **142**, 105–110.

31 X. Y. Xue, L. Xing, Y. Chen, S. Shi, Y. Wang and T. Wang, *J. Phys. Chem. C*, 2008, **112**, 12157–12160.

32 S. Choi, A. Katoch, J. Zhang and S. S. Kim, *Sens. Actuators, B*, 2013, **176**, 585–591.

33 S. W. Choi, J. Zhang, K. Akash and S. S. Kim, *Sens. Actuators, B*, 2012, **169**, 54–60.

34 V. Kumara, S. Sen, K. P. Muthe, N. K. Gaur, S. K. Gupta and J. V. Yakhmi, *Sens. Actuators, B*, 2009, **138**, 587–590.

35 L. Liu, T. Zhang, L. Y. Wang and S. C. Li, *Mater. Lett.*, 2009, **63**, 2041–2043.

36 F. Shao, M. W. G. Hoffmann, J. D. Prades, R. Zamani, J. Arbiol, J. R. Morante, E. Varechkina, M. Rumyantseva, A. Gaskov, I. Giebelhaus, T. Fischer, S. Mathur and F. Hernández-Ramírez, *Sens. Actuators, B*, 2013, **181**, 130–135.

37 M. Verma, A. Chowdhuri, K. Sreenivas and V. Gupta, *Thin Solid Films*, 2010, **518**, E181–E182.

38 Z. Xu, G. Duan, Y. Li, G. Liu, H. Zhang, Z. Dai and W. Cai, *Chem.–Eur. J.*, 2014, **20**, 6040–6046.

39 N. V. Toan, N. V. Chien, N. V. Duy, D. D. Vuong, N. H. Lam, N. D. Hoa, N. V. Hieu and N. D. Chien, *Appl. Surf. Sci.*, 2015, **324**, 280–285.

40 K. I. Choi, H. J. Kim, Y. C. Kang and J. H. Lee, *Sens. Actuators, B*, 2014, **194**, 371–376.

41 M. K. Verma and V. Gupta, *Sens. Actuators, B*, 2012, **166–167**, 378–385.

42 P.-P. Zhang, H. Zhang and X.-H. Sun, *Nanoscale*, 2016, **8**, 1430–1436.

43 M. A. Andio, P. N. Browning, P. A. Morris and S. A. Akbar, *Sens. Actuators, B*, 2012, **165**, 13–18.

44 J. H. Lee, *Sens. Actuators, B*, 2009, **140**, 319–336.

45 X. X. Xu, J. Zhuang and X. Wang, *J. Am. Chem. Soc.*, 2008, **130**, 12527–12535.

46 W. Guo, X. C. Duan, Y. Shen, K. Z. Qi, C. Y. Wei and W. J. Zheng, *Phys. Chem. Chem. Phys.*, 2013, **15**, 11221–11225.

47 Y. Ren, Z. Ma and P. G. Bruce, *Chem. Soc. Rev.*, 2012, **41**, 4909–4927.

48 W. Li and D. Y. Zhao, *Chem. Commun.*, 2013, **49**, 943–946.

49 Y. Teng, L. X. Song, A. Ponchel, Z. K. Yang and J. Xia, *Adv. Mater.*, 2014, **26**, 6238–6243.

50 Y. Teng, L. X. Song, A. Ponchel, E. Monflier, Z. C. Shao, J. Xia and Z. K. Yang, *RSC Adv.*, 2014, **4**, 26847–26854.

51 A. Lannoy, R. Bleta, C. Machut, E. Monflier and A. Ponchel, *RSC Adv.*, 2014, **4**, 40061–40070.

52 J. Zhao, W. N. Wang, Y. P. Liu, J. M. Ma, X. W. Li, Y. Du and G. Y. Lu, *Sens. Actuators, B*, 2011, **160**, 604–608.

53 T. Becker, S. Ahlers, C. Braunmuhl, G. Muller and O. Keisewetter, *Sens. Actuators, B*, 2001, **77**, 55–58.

54 Y. Yang, C. G. Tian, J. C. Wang, L. Sun, K. Y. Shi, W. Zhou and H. G. Fu, *Nanoscale*, 2014, **6**, 7369–7378.

55 J. Zhang, S. Wang, Y. Wang, M. Xu, H. Xia, S. Zhang and S. Wu, *Sens. Actuators, B*, 2009, **139**, 411–417.

56 Y. Yang, L. Sun, X. T. Dong, H. Yu, T. T. Wang, J. X. Wang, R. H. Wang, W. S. Yu and G. X. Liu, *RSC Adv.*, 2016, **6**, 37085–37092.

57 S. J. Choi, S. Chattopadhyay, J. J. Kim, S.-J. Kim, H. L. Tuller, G. C. Rutledge and I.-D. Kim, *Nanoscale*, 2016, **8**(17), 9159–9166.

58 S. Z. Deng, V. Tjoa, H. M. Fan, H. R. Tan, D. C. Sayle, M. Olivo, S. Mhaisalkar, J. Wei and C. H. Sow, *J. Am. Chem. Soc.*, 2012, **134**, 4905–4910.

59 Z. Y. Zhang, R. J. Zou, G. S. Song, L. Yu, Z. G. Chen and J. Q. Hu, *J. Mater. Chem.*, 2011, **21**, 17360–17366.

60 Y. Yang, C. G. Tian, L. Sun, R. J. Lu, W. Zhou, K. Y. Shi, K. Kan, J. C. Wanga and H. G. Fu, *J. Mater. Chem. A*, 2013, **1**, 12742–12749.